Journal of Structural Geology 48 (2013) 33–44

Contents lists available at SciVerse ScienceDirect

Journal of Structural Geology

journal homepage: www.elsevier.com/locate/jsg

Enabling 3D geomechanical restoration of strike- and oblique-slip faults using geological constraints, with applications to the deep-water Niger Delta

Pauline Durand-Riard [a,*], John H. Shaw [a], Andreas Plesch [a], Gbenga Lufadeju [b]

[a] Structural Geology and Earth Resources Group, Harvard University, 20 Oxford Street, Cambridge, MA 02138, USA
[b] Department of Petroleum Resources, Ministry of Oil, Nigeria

ARTICLE INFO

Article history:
Received 8 June 2012
Received in revised form
1 November 2012
Accepted 11 December 2012
Available online 26 December 2012

Keywords:
Geomechanical restoration
Strike-slip faults
Boundary conditions
Implicit approach

ABSTRACT

We present a new approach of using local constraints on fault slip to perform three-dimensional geomechanical restorations. Geomechanical restoration has been performed previously on extensional and contractional systems, yet attempts to restore strike- and oblique-slip fault systems have generally failed to recover viable fault-slip patterns. The use of local measures of slip as constraints in the restoration overcomes this difficulty and enables restorations of complex strike- and oblique slip-systems. To explore this approach, we develop a synthetic restraining bend system to evaluate different ways that local slip constraints can be applied. Our restorations show that classical boundary conditions fail to reproduce the fault offset and strain pattern. In contrast, adding piercing points and/or properly constraining lateral walls enables restoration of the structure and resolves the correct pattern of slip along the faults. We then restore a complex system of tear-faults in the deepwater Niger Delta basin. We use channel offsets imaged by the seismic data to define local fault-slip constraints. Balancing these constraints equally on both sides of the major faults yields the most consistent restoration outcomes. This approach resolves reasonable slip styles on the complex set of thrust, normal, and strike-slip faults in the structure. This suggests that limited geologic fault slip constraints can be effectively incorporated in geomechanical restorations, yielding accurate restoration kinematics and thereby forecasting faults slip patterns within the structures.

1. Introduction

Structural restoration is a primary tool used to validate structural interpretations and reconstruct the deformation histories of faults and folds. In the last decade, restoration of cross-sections (Dahlstrom, 1969), maps (Gratier and Guillier, 1993; Rouby, 1994; Rouby et al., 2000; Massot, 2002), or volumes (De Santi et al., 2002; Muron, 2005; Maerten and Maerten, 2006; Moretti et al., 2006; Guzofski et al., 2009; Durand-Riard et al., 2010) has been successfully applied to complex thrust or normal fault systems, leading to an improved understanding of the spatial and temporal development of geological structures. These restorations have many applications, from defining the amounts of shortening or extension in a region, to the assessment of the timing of hydrocarbon trap development. However, when it comes to strike- or oblique-fault systems, the application of the restoration method is more challenging.

Indeed, cross-section restoration, based on geometric criteria such as conservation of line length, area, or angle, is inherently two-dimensional (Chamberlin, 1910; Dahlstrom, 1969). Thus, its application to strike- and oblique-slip fault systems is limited. Map restoration, as well as kinematic volume restoration, is similarly based on geometric assumptions and most of the methods require that fault offsets to be specified (Gratier and Guillier, 1993; Rouby, 1994; Rouby et al., 2000; Massot, 2002). In natural settings, the fault slip is often not known everywhere, making the application of such methods to strike- and oblique-slip faults difficult. In new approaches of 3D geomechanical restoration (De Santi et al., 2002; Muron, 2005; Maerten and Maerten, 2006; Moretti et al., 2006; Durand-Riard et al., 2010), global kinematic rules are not required, and a mechanically stable restoration is performed that considers rock properties. In these methods, the fault offset is a result of the computation rather than being specified by the user. This makes these methods a better framework for investigating the displacement patterns of complex faults, such as in strike- and oblique slip

* Corresponding author. Tel.: +1 617 496 1386; fax: +1 617 495 7660.
E-mail addresses: durandriard@fas.harvard.edu (P. Durand-Riard), shaw@eps.harvard.edu (J.H. Shaw), plesch@fas.harvard.edu (A. Plesch), gblufadeju@hotmail.com (G. Lufadeju).

0191-8141/$ – see front matter © 2013 Elsevier Ltd. All rights reserved.
http://dx.doi.org/10.1016/j.jsg.2012.12.009

systems. However, applying this restoration approach using classical boundary conditions (flattening of a geologic datum horizon) to strike- and oblique-slip faults does not lead to satisfactory results. Specifically, such restorations generally do not recover the proper amounts of strike-slip, and as a result impose unreasonably high rock strains and invalid fold kinematics. In this paper, we develop a new approach to using local geologic fault slip constraints, such as piercing point offsets, to guide 3D geomechanical restorations. We first investigate these new constraints by restoring a synthetic restraining bend model including a fold above an oblique-slip fault that connects two vertical right-lateral strike-slip faults using different sets of boundary conditions. We then restore a natural structure located in the outer fold-and-thrust belt of the deep-water Niger Delta basin, where the shortening due to the sliding on the shelf is accommodated not only by thrust fault systems (Doust and Omatsola, 1990; Wu and Bally, 2000; Bilotti and Shaw, 2005; Corredor et al., 2005), but also by tear-faults, mostly parallel to the transport direction (Benesh, 2010). We focus on the deformation induced by these specific right-lateral strike-slip faults within one restraining and releasing bend structure. The quality of the 3D seismic data allows us to investigate the complexity of this system and to build a detailed structural model. The restoration of this model using only the flattening of the top horizon leads to an inconsistent sense of strike-slip. Thus, we identify channels offsets using the seismic data, allowing us to constrain the restoration of the strike-slip faults. While the focus of this paper is strike-slip faults, we suggest that using such geological constraints is also helpful for restoring any inherently 3D structures, such as those with faults of different orientations or styles (Durand-Riard, 2010; Lovely et al., 2010; Lovely, 2011; Durand-Riard and Shaw, 2012).

2. Developing a strike-slip fault restoration workflow

2.1. 3D geomechanical restoration overview

We use a Finite Element Method based geomechanical restoration approach that employs volume preservation and energy minimization constraints (De Santi et al., 2002; Muron, 2005; Maerten and Maerten, 2006; Moretti et al., 2006; Guzofski et al., 2009; Durand-Riard et al., 2010). This method allows for a precise description of the deformation of geologic structures through time while accounting for rock strength contrasts between and within the layers.

Performing FEM-based geomechanical 3D restoration requires several steps (Fig. 1): (i) discretizing the stratigraphic units using a tetrahedral mesh. This mesh is topologically discontinuous across faults, which allows slip to occur between the hanging and the footwall; and (ii) defining elastic geomechanical properties. Typically, these properties are isotropic, characterized by two elastic parameters (Young's modulus and Poisson's ratio, or Lamé's coefficients).

When growth strata are available, the restoration can be performed sequentially, layer after layer: once a layer is restored, it is removed and the underlying unit can be restored. For each layer, specific displacement and contact conditions are defined. These conditions can include: flattening of the top horizon, setting one or more regions to a known location in order to ensure the uniqueness of the solution (Muron, 2005), and ensuring fault compliance with contact conditions (Wriggers, 2002).

In response to these boundary conditions, the tetrahedral elements deform iteratively until equilibrium is reached and the strain energy of restoration is minimized. The displacement vectors for each model element are calculated using the Finite Element Method (Zienkiewicz, 1977; Muron, 2005; Maerten and Maerten, 2006; Moretti et al., 2006), combined with a dynamic relaxation algorithm (Underwood and Park, 1978; Papadrakakis, 1981; Oakley and Knight, 1995) that allows for handling complex fault networks (Muron, 2005). The strain tensor is computed in 3D for every tetrahedron, providing a description of the deformation throughout the model.

Given the limits of the simple constitutive laws that are used in the restoration and the fact that far-field stress is not accounted for in the computation, the calculated strain values are unlikely to provide a precise description of internal rock state. Nevertheless, a number of studies have shown that these calculated values can be used to describe how strains are distributed throughout a structure both in orientation and relative magnitude (Maerten and Maerten, 2006; Moretti et al., 2006; Plesch et al., 2007; Guzofski et al., 2009; Durand-Riard and Shaw, 2012; Vidal-Royo et al., 2011), thus providing meaningful information about the deformation history. In this context, it is considered useful to analyze the significant invariants of the strain tensor, which can be computed from the restoration strains. These invariants include the dilation (first invariant of the strain tensor) and the distortion (second invariant of the deviatoric strain tensor).

This approach has been previously applied to a number of kinematic and natural structures (Müeller et al., 2005; Muron, 2005; Plesch et al., 2007; Guzofski et al., 2009; Suess et al., 2009; Titeux, 2009; Durand-Riard et al., 2010; Plesch et al., 2010; Durand-Riard et al., 2011; Durand-Riard and Shaw, 2012), serving many purposes such as (i) improving the understanding of complex systems by defining fault and fold kinematics and assessing timing and magnitude of deformation; and (ii) helping fracture prediction by estimating strain distributions. Few 3D restorations of oblique- and strike-slip structures have been performed, as attempts to restore such structures have not been able to resolve reasonable fault-slip patterns.

2.2. Strike-slip fault restoration

To explore the most effective way of constraining geomechanical restorations of strike- and oblique-slip systems, we construct a balanced model of a restraining bend structure. This model includes an uplift and a fold that grew by kink-band migration above an oblique-slip fault that connects two vertical, right-lateral strike-slip faults (Fig. 2) (Shaw et al., 1994). This model is not intended to

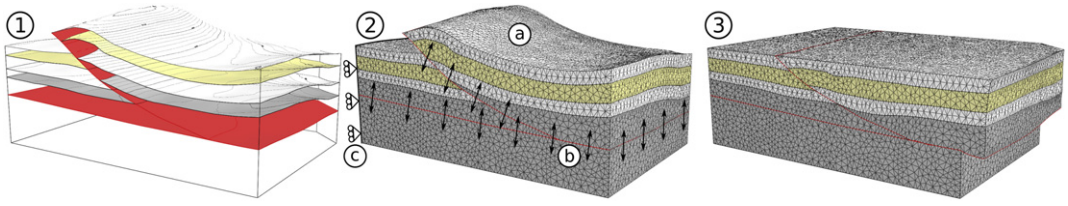

Fig. 1. Volume restoration workflow: 1) Initial structural model; 2) Conforming tetrahedral mesh with topological regions, in which mechanical properties of the rocks are assigned per layer. The boundary conditions are shown on the model: a) the topmost horizon is flattened; b) contacts are defined at the fault surfaces to ensure there is no gap or overlap at the end of the restoration; and c) one wall is fixed along its normal direction; 3) Restored model. Initial model of surfaces courtesy of Chevron.

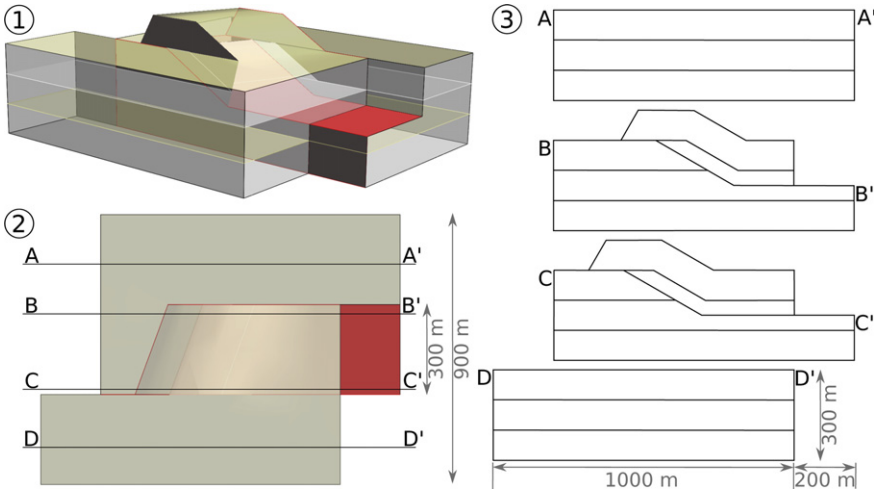

Fig. 2. Synthetic model of the restraining bend: 1. Surface model showing a kink band fold above an oblique-slip fault that connects two vertical right-lateral strike-slip faults; 2. Map view of the model, displaying the location of the cross-sections shown in 3.

describe the full range of deformation styles that occur in strike-slip systems. Rather, it provides a useful target for 3D restoration that includes both dip and strike-slip faults, and folding related to displacement gradients on these faults. The maximum offset of these strike-slip faults is 200 m, producing a maximum uplift of 100 m above the thrust. The "restored" model (the theoretical undeformed model) is a cuboid with a 900 × 1000 square meters base, where the thrust is located in the middle of the 900 m side and is 300 m wide (Fig.2).

We test three different sets of boundary conditions in restoring this model, in order to assess which boundary conditions work best for strike- and oblique slip fault systems (Fig. 3). In essence, these three sets of boundary conditions reflect different ways of incorporating geological constraints in the restorations. The classical conditions require flattening a geologic horizon and fault compliance, which are generally applied in all types of restorations. The second case adds geologic insights, by defining the slip on the faults at one or more locations. These fault slip constraints could be informed by local piercing point observations. The third set of boundary conditions also imposes fault slip constraints, but does so on model walls rather than at specific locations along the faults. The goal of testing these different sets of boundary conditions is to ascertain what types of geological constraints are needed, and how they should be imposed, to yield the most meaningful geomechanical restorations.

In details, the following boundary conditions are applied:

- Classical boundary conditions, which involve flattening the topmost horizon and ensuring fault compliance (i.e., ensuring that no gaps develop between fault surfaces). The lateral walls in the model are parallel to the strike-slip faults, and are allowed to move only parallel to themselves. That is, they cannot move orthogonally to the strike-slip faults. The undeformed footwall block is defined as the master side for the fault contact condition, such that this block does not move at the fault compliance step during the restoration (only the slave side moves to be set in contact with the master; see Wriggers (2002); Muron (2005) and Durand-Riard (2010) for more details).
- Adding piercing points that locally constrain the slip along the strike-slip fault. To apply this condition, the mesh is modified so that the distance between the two considered mesh nodes corresponds to the input offset. A tied nodes condition is then set on these nodes. This condition ensures the nodes are in contact in the restored state.
- Adding displacement condition on the back-wall, corresponding to the reverse displacement tectonic settings (the displacement along x is set to 200 m). This differs from the previous set of boundary conditions as the fault offset is constrained along a model boundary rather than at a single point along the fault.

We use a default homogeneous sandstone material for the restorations of this model (Young's modulus $E = 15$ GPa and Poisson's ratio $\nu = 0.31$).

2.3. Results and discussion

All three sets of boundary conditions that we tested yielded restoration outcomes that flattened the datum horizon and

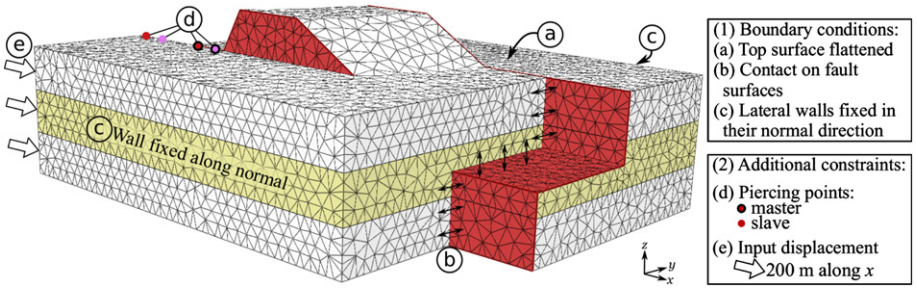

Fig. 3. Different sets of boundary conditions used for the restoration: (1) the basic set of boundary conditions; (2) the basic set plus piercing points (d); or the basic set plus an input displacement applied to the back-wall (e).

maintained fault compliance. Fig. 4 shows the restoration results, in terms of geometry and dilation distribution, for these three different sets of boundary conditions.

First, using only the classical conditions, we can see that the fault slip is not fully recovered (95 m for the first, and 151 m for the second strike-slip fault; in contrast, both have an input slip of 200 m). Moreover, the deformation (strain) is distributed in the horizontally translated block (block B in Fig. 4), rather than being localized in the uplifted and folded block (block A in Fig. 4) as expected. Thus, this result yields only a partially restored structure, and does a poor job of recovering fault slip and strain patterns.

Adding piercing point along one of the strike-slip faults globally enhances the restoration results. The faults slip recovery is improved: adding piercing points yields 130 and 169 m of slip on the two strike-slip segments. This is closer to the input slip value of 200 m than was the previous restoration with no fault slip constraints. The piercing point constraints also decrease the extension that occurs in block A, which is expected to have no deformation. Ideally, the horizontally translated blocks in our kinematic model are moving without being deformed: it is a rigid body translation. However, the piercing point nodes induce localized high deformation. This is inherent to the use of localized constraints in geomechanical restoration. Indeed, a contact condition is set between two nodes that are located relatively far away from each other in the initial configuration, thus imposing a significant displacement on the hangingwall node. Because the geomechanical restoration is based on an energy minimization and not on rigid body rotation/translation, this leads to a high deformation in the area of the constrained nodes.

In contrast, constraining the backwall so that its displacement is equal to the total slip (200 m) leads to very good restoration results: almost all the slip is recovered for both faults (184 and 196 m), and the deformation is concentrated in the folded and uplifted block (block A). No significant deformation appears elsewhere in the model. Also, the underlying horizons, which were not assigned any constraint, are almost flattened and the dip-slip has been recovered in a better way than with the other constraints. From a computational point of view, imposing the displacement on a wall allows distributing the constraint on numerous nodes. In response to this constraint, the nodes are displaced and the deformation is propagated from node to node through the entire system. When the geological constraint is assigned only on a few nodes as it is when using one or more piercing points along the faults, the deformation cannot be fully propagated throughout the system, hence leading to high strain around those nodes.

2.4. New restoration workflows

As demonstrated in the model restoration results, using only classical boundary conditions does not lead to satisfactory results in terms of slip recovery and deformation distribution. Using piercing points constraints improves the restoration, but the most satisfactory results are provided when the complete displacement on the back-wall of the model is constrained. In the case of a complex natural case study, however, this back-wall condition may be hard to determine, because the slip is not known everywhere and in fact may vary along the borders of the model. Bearing that in mind, two approaches can be considered, depending on the objectives of the restoration:

- Use of piercing points: While not yielding the best outcome in our model restoration, the slip recovery is better than using only the classical boundary conditions. Moreover, the distribution of strain in the model is perhaps qualitatively realistic, except for localized strain around these particular constrained points. These restorations could be further improved by using more piercing points along the fault, and, ultimately, by constraining the whole fault line with known direction or vectors of slip. This would allow for a realistic fault slip and strain distribution without over-constraining the restoration.

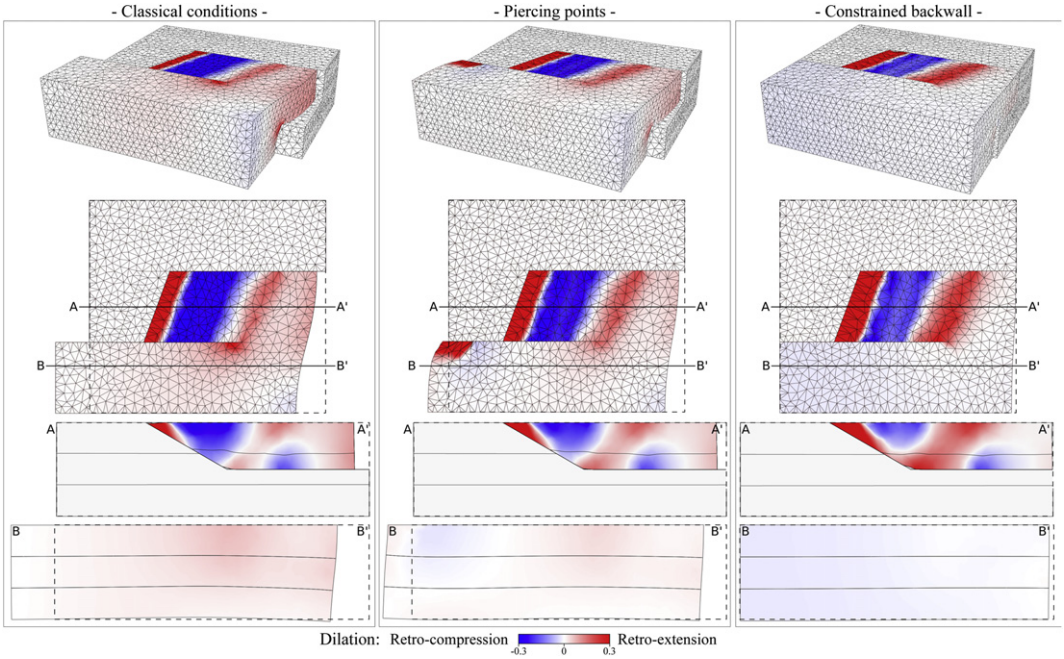

Fig. 4. Restoration results with the different sets of boundary conditions, showing, from top to bottom, the restored state of the model, a map view of the restored model, a vertical section in the faulted and uplifted block (AA'), referred to as block A in the text, and a vertical section in the horizontally translated block (BB'), referred to as block B in the text. All the models and sections are painted with the retro-dilation property (computed from the current, deformed state to the restored state). The dashed lines correspond to the ideal restored state, where all slip is recovered.

- Use of displacement constraints on one or several model borders, where the slip is known from local piercing points constraints. This allows for the resolution of differential slip on the faults in case of relays or numerous faults, while yielding a realistic pattern of deformation. In cases where appropriate boundary displacements are not known, a range of possible values could be tested and evaluated based on the resolved slip and strain patterns.

To investigate the application of these new approaches, we perform restorations of a complex natural structure in the deepwater Niger Delta. This structure includes strike- and dip-slip faults with both restraining and releasing bend architectures. The high-quality 3D seismic reflection data in the region allows for a detailed interpretation of the fault network and mapping of channel offsets that can be used as constraints for the restoration.

3. Three-dimensional modeling of a complex system in the northern Niger Delta

3.1. Geological settings

The Niger Delta, one of the largest progradational deltas in the world (Doust and Omatsola, 1990), is located in the Gulf of Guinea on the margin of West Africa. It can be described by four primary structural zones (Connors et al., 1998; Corredor et al., 2005) as shown in Fig. 5, including: an extensional province; the inner fold and thrust belt; a transitional detachment fold zone; and the outer fold-and-thrust belt. Our area of interest straddles the outer fold-and-thrust belt and the detachment fold zone. Contraction is caused by gravity-driven extension updip on the shelf and shortening is mostly accommodated by thrust faults and fault-related folds. Near the northern termination of the outer fold-and-thrust belt, it has been shown that tear-faults also play an important role (Benesh, 2010).

In our region of interest, three right-lateral strike-slip faults trend NE-SW, parallel to the transport-direction (Fig.5B). They are rooted at depth into the same detachment level as the thrust faults. The detachment beneath the structures that we will model is interpreted to have formed at the boundary between the Akata shales and the overlying Agbada Formation. These tear-faults show nearly vertical dips along most of their extents. However, significant changes in fault dip occur in regions of fault step-overs, resulting in localized extensional releasing bends and contractional restraining bends. In this study, we focus on a system including a restraining and a releasing bend, located on the eastern part of the southernmost tear-fault (Fig.5C). The deformation in this area appears to be independent from the major thrust faults mapped in the area, making it a suitable study site for testing strike-slip restoration approaches.

3.2. Interpreted structures

We use 3D seismic data (see Fig.5A for location) to constrain the faults geometry. Detailed interpretations were made on both depth slices and vertical sections leading to a structural model where the tear-faults are described as several relaying fault segments along strike, surrounded by numerous shallower faults interpreted as reverse or normal faults. Our structural model includes more than 50 faults (Fig. 6). Along strike (NE–SW), eight strike-slip faults are relaying with each other; at the extremities of our model some of them are laterally merging onto each other. Starting from the SW, the first five strike-slip faults dip steeply toward the SE (average dip of 83°), while the three faults in the NE dip steeply toward the SW (average dip of 87°). The relative positions of these faults along strike produce two major step-overs: a left step, creating

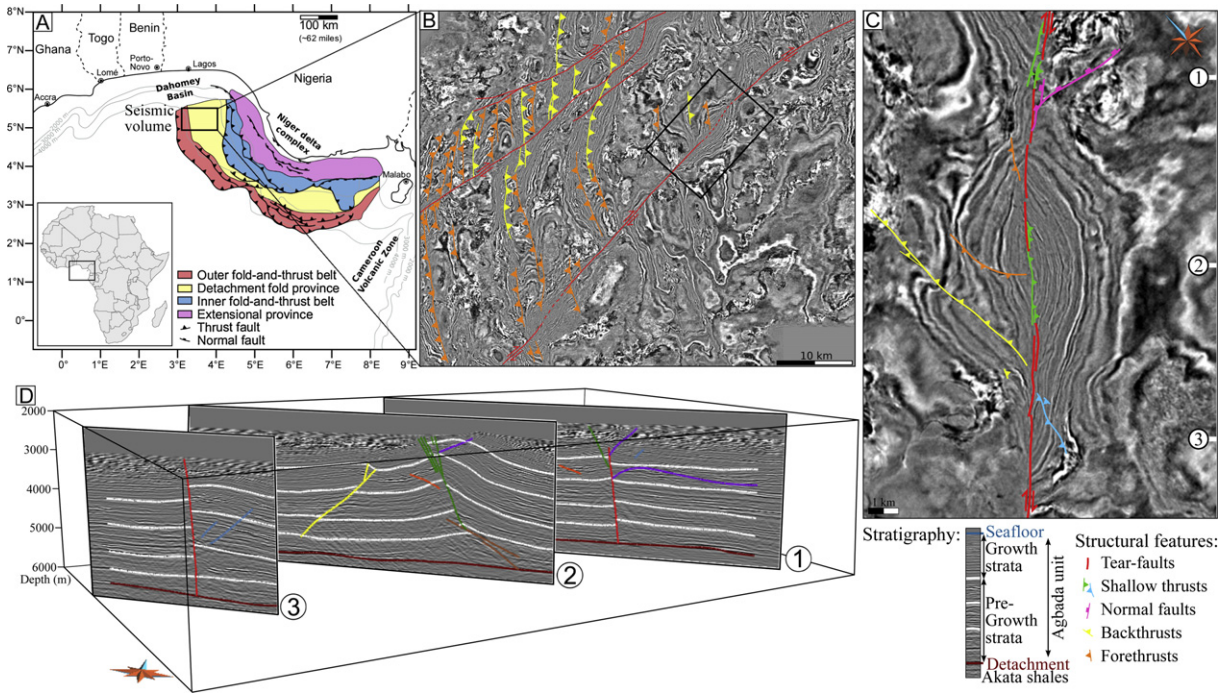

Fig. 5. A. Generalized structural map of the main provinces of the Niger Delta and location of the 3D seismic reflection data volume used in this study. Modified after Benesh (2010). B. Depth slice showing the three primary tear-faults and some thrust faults (seismic interpretation by Benesh (2010)). The dashed line along the southernmost tear-fault corresponds to a region of fault step-over. The studied system is boxed. C. Zoom in study area and location of the vertical sections. D. Vertical depth sections along the restraining bend, with interpreted faults and horizons. Seismic data provided courtesy of Department of Petroleum Resources, Ministry of Oil, Nigeria.

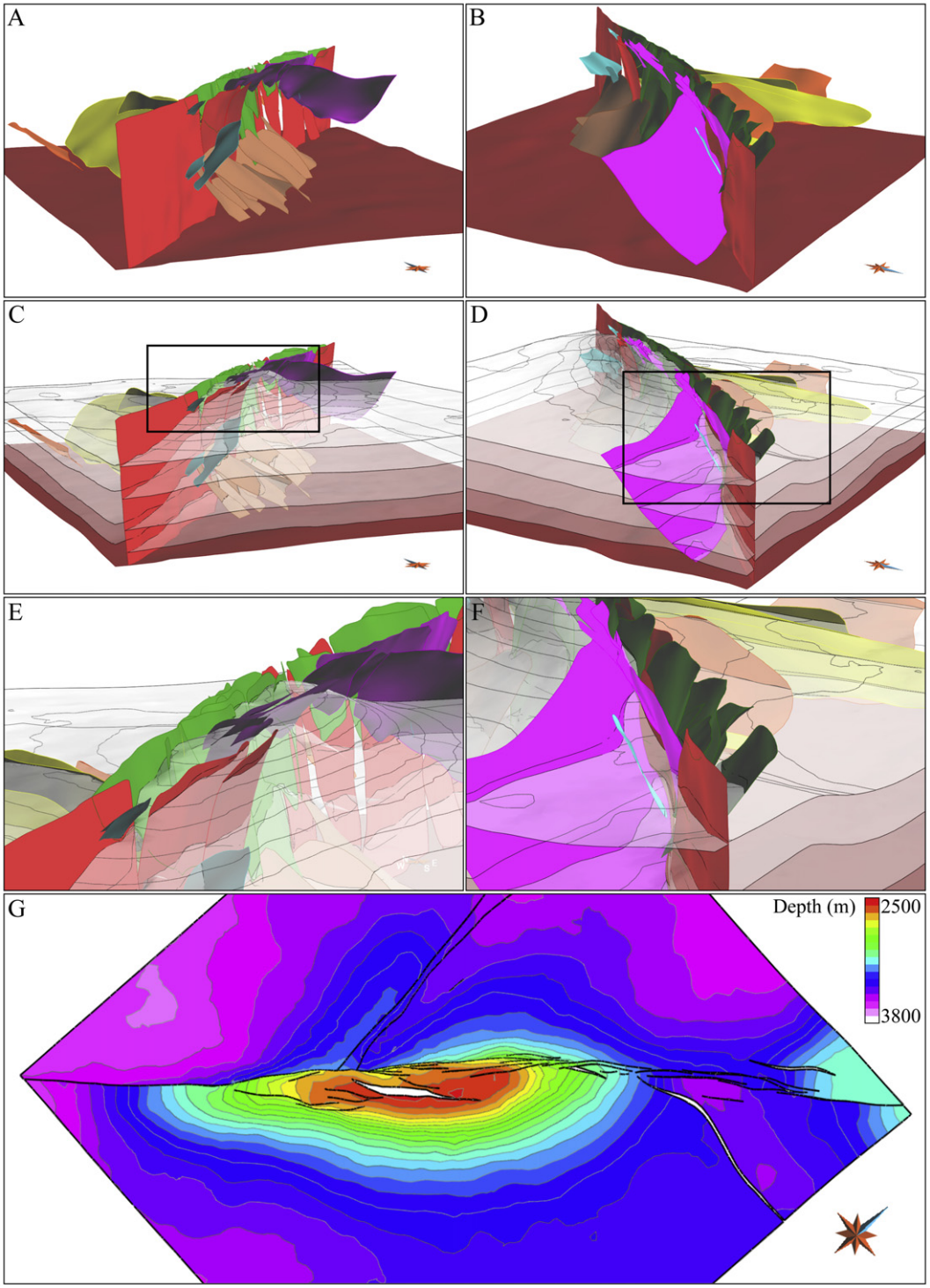

Fig. 6. A and B) Interpreted fault network corresponding to the area boxed in Fig. 5C, viewed from the SW and the NE, respectively (for color keys, see Fig. 5); C and D) Structural model showing four interpreted horizons, corresponding to prominent markers in the seismic data. The topmost horizon has the contours of depth; E) Zoom on the uplift at the center of the restraining bend; F) Zoom on the releasing bend; and G) Map view of the top horizon with the fault traces, contoured by depth. (For interpretation of the references to colour in this figure legend, the reader is referred to the web version of this article.)

a restraining bend with local folding and uplift; and a right step, producing a releasing bend bounded by a large normal fault.

Outside of the restraining bend, the strike-slip faults root into the detachment at depth, and are thus referenced to as tear-faults hereafter (see cross-sections in Fig. 5D). At the center of the restraining bend (Fig. 6E), the complexity of the fault system increases: at shallow depth, in the uplift, sixteen SE dipping thrust faults accommodate some of the displacement and six small NW dipping normal faults accommodate local extension in the outer-arc of the uplift. Some of the thrusts terminate onto deeper SE dipping thrust faults. These nine thrusts exist only below 4000 m of depth and sole onto the detachment. In addition to this complex system in the restraining bend, five N–S oriented thrust faults are also present on the NW side of the bend. In the releasing bend

(Fig. 6F), three relaying tear-faults separate a set of four shallow normal faults present on the SE side of the bend from eight shallow thrusts on the NW side. A larger normal fault separates the releasing bend from the restraining bend.

In addition to the fault network, several horizons have been interpreted, corresponding to prominent seismic reflectors (Fig. 6) in the pregrowth strata. The horizons were mapped using both autocorrelation and standard interpretation techniques, and were iterated to produce reasonable fault displacement gradients. The horizon mapping reveals a significant vertical offset (up to 600 m) in the restraining bend, whereas the maximum vertical offset (up to 200 m) is relatively small in the releasing bend.

3.3. Strike-slip offsets

In this part of the delta, numerous channels are present and clearly imaged on the seismic data, on time and depth slices. In order to constrain the restoration, we look for channel offsets on horizons. However, the initial interpreted horizons correspond to prominent and continuous reflectors and were chosen so that they are not affected by channels for an easier interpretation. Other horizons have to be extracted for channels imaging purpose. Using the implicit approach (Frank et al., 2007; Caumon et al., 2007), the interpreted horizons are used to constrain the interpolation of a stratigraphic property (Fig. 7A). This property is continuous between two horizons (Fig. 7B), which allowed extracting as many isosurfaces as desired (example of extracted isosurface in Fig. 7C). Numerous isosurfaces were extracted, about every 10 m vertically. The seismic amplitude was mapped onto the extracted horizons. We selected a range of depth where channels are imaged and seem to be offset by the tear-faults. At these locations, most of the channels are not single features but stacked on each other. To facilitate our analysis, we drew every distinctive channel over a relatively large range of depth (about 200 m), and then we interpreted the offsets of the channel systems (Fig. 8).

This workflow allows us defining two strike-slip constraints: 462 m of dextral slip on the NE end of the model, and 831 m of dextral slip on the SW end. This increasing amount of slip in the transport direction is consistent with tear-fault displacement patterns (Benesh, 2010).

4. Restorations of the natural system

4.1. From the structural model to a restoration model

To perform restorations, the structural model needs to be simplified in order to meet the meshing requirements. These simplifications should respect the geometry of the restraining and releasing bends. To accomplish both of these goals, we simplified the model as follows:

- The major relaying tear-faults were kept, while the small ones were merged together when they have similar dip. The resulting model contains six subvertical faults along strike (versus eight in our initial interpretation).
- Some of the deep thrusts were merged together, when they have a similar dip and strike, which led to three faults (versus six).
- In the outer-arc of the uplift, one normal fault was included, that respects the dip, strike and dimensions of the interpreted shallow normal faults. On the NW side of the restraining bend, one thrust fault was included, which is consistent with the dimensions and orientation of the interpreted shallow thrust faults.
- In the releasing bend, the major bounding normal fault was included, as well as one shallower normal fault and one thrust, respectively on the SE and NW side of the bend.
- On the NW side of the bend, only the largest NW–SE oriented backthrust was included, because the other back and fore-thrusts have very small offsets.

These simplifications lead to a final model including fifteen faults (Fig. 9). We then needed to define the topology of this fault network. Several models were built and analyzed, and we chose to restore the solution that minimized the branching between the faults where the seismic data failed to accurately define it. To achieve this, we relied on the geometry of the interpreted horizons to evaluate fault branches. A stratigraphic property corresponding to the interpreted horizons is interpolated in the model, following the approach described in Section 3.3 and illustrated by Fig. 7, and the faults are branched according to the geometry of the interpolated horizons. For example, when two faults are branched but this is mistakenly not included in the fault network, the resulting horizon cannot be correct. In that case, two interpreted points belonging to a horizon are close to each other horizontally but have very different elevations. Because the two faults are not branched in the model, there is no discontinuity between the two points, leading to an implicit horizon with a ungeologic shape, or "bubbles". When this happens, we branch the two faults so that there is a discontinuity in the model. Following this strategy, we end with a model where the tear-faults are branched laterally in the releasing bend and at the lateral boundaries of the model, but not within the restraining bend.

This model is discretized with tetrahedra, and the meshed stratigraphic units are assigned geomechanical properties. In this area of the Niger delta, the detachment is interpreted as occurring

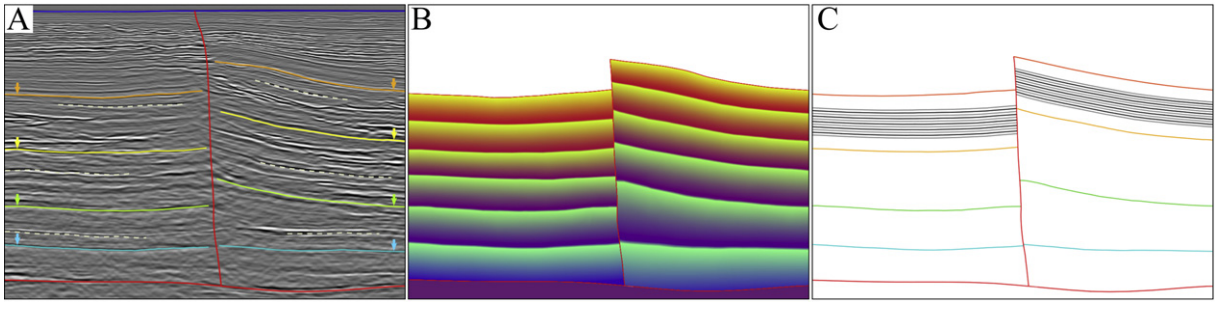

Fig. 7. A) Seismic section and interpreted horizons, used as control points for the interpolation of the stratigraphic property (solid lines). Additional "isolines" constraints are used when features can be interpreted but don't belong to any interpreted horizon (dashed lines). To ensure the continuity of the property, a constraint on the constant gradient is set. B) Interpolated stratigraphic property. C) Extracted horizons. The continuity of the property allows extracting stratigraphic surfaces between interpreted horizons. Seismic data provided courtesy of Department of Petroleum Resources, Ministry of Oil, Nigeria.

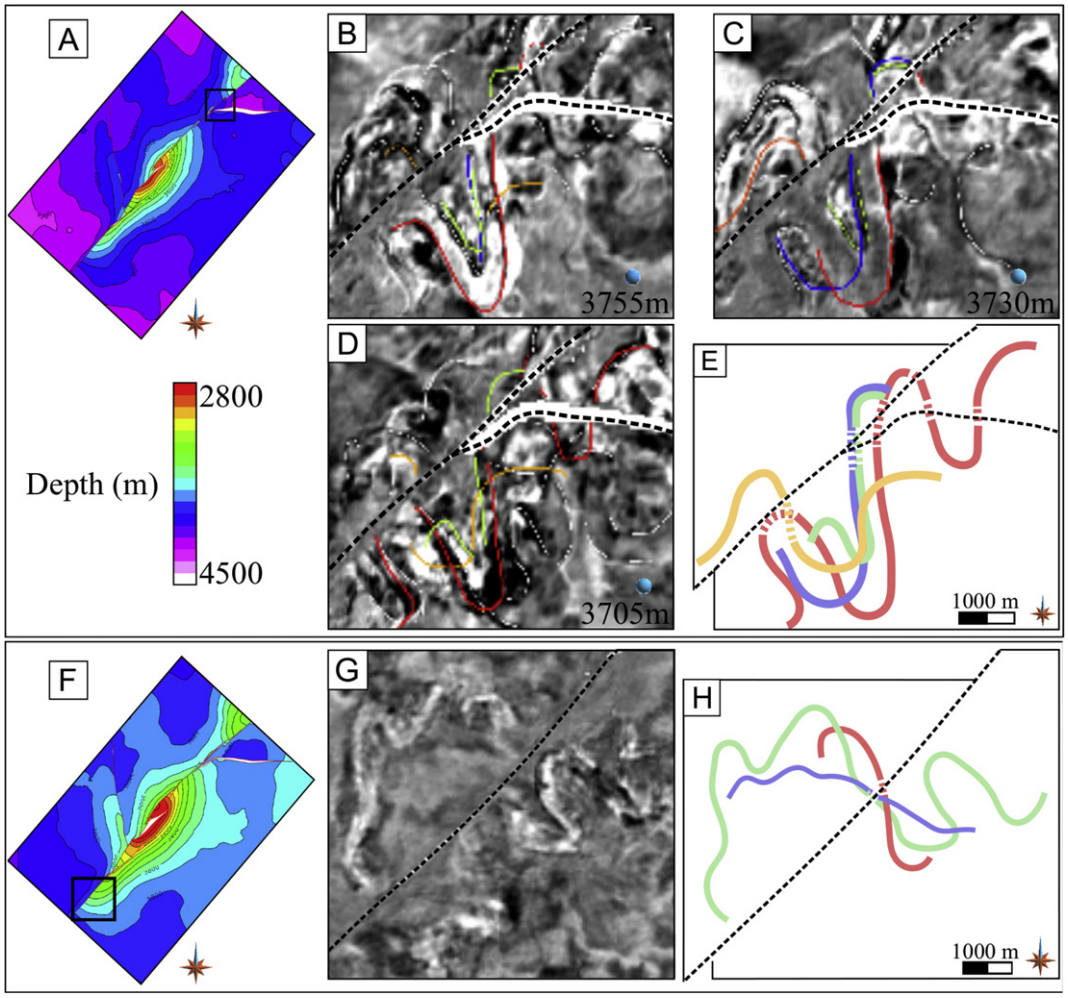

Fig. 8. A) One extracted horizon, contoured by depth, showing the location of boxes B to E. B–D) interpreted channel features on some of the extracted horizons, colored with the seismic amplitude. E)"Restored" interpreted channels. The corresponding offset is 462 m. F) Another extracted horizon, at a different depth, showing the location of boxes G and H. G) One horizon colored with the seismic amplitude, showing clearly imaged channels. H) "Restored" horizon. The corresponding offset is 839 m. Seismic data provided courtesy of Department of Petroleum Resources, Ministry of Oil, Nigeria.

above or at the contact between the Akata shales unit and the Agbada Formation (Benesh, 2010). Above the detachment, geomechanical properties corresponding to the Agbada Formation are assigned: a Young's modulus $E = 15$ GPa and a Poisson's ratio $\nu = 0.31$. Below the detachment a much weaker material, corresponding to the Akata shales, is set with $E = 1.4$ GPa and $\nu = 0.40$ (Guzofski et al., 2009). These values are probably not representative of all of the lithologies in the study area, but we felt that it was appropriate to use a single, representative value so that we could isolate the effects of the different boundary conditions in our restorations. Moreover, the limit between Akata and Agbada being located at the detachment, there isn't any contrast of mechanical

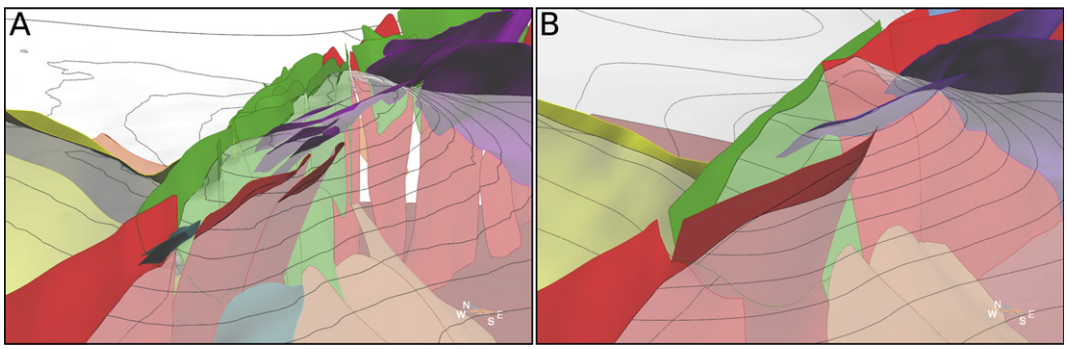

Fig. 9. A. Restraining bend as in the interpreted structural model; B. Simplified model used for the restorations. See Fig. 5 for color keys. The table summarizes the simplifications. T stands for thrust, N for normal fault, F for forethrust and B for backthrust. (For interpretation of the references to colour in this figure legend, the reader is referred to the web version of this article.)

properties in the part that undergoes deformation. The use of different values for the Young's modulus and Poisson's ratio would therefore not impact the strain distribution but only the absolute values of the invariants.

4.2. Restoration using classical boundary conditions

We first restore our model using only classical boundary conditions. In this case, the top horizon is flattened and the lateral walls are allowed to move only parallel to themselves. Fault contacts are set so that there is no gap or interpenetration in the restored configuration. As for the synthetic case, using only the classical boundary conditions doesn't reproduce the expected strike-slip patterns. At the NE extremity of the model, although the correct sense of slip on the faults is assessed, the recovered fault offsets don't match the channel offsets. The recovered slip is about 525 m, where the channels offsets define 462 m of strike-slip. At the SW extremity of the model, both hangingwall and footwall of the tear-faults move toward the SW, with about 80 m of sinistral strike-slip. The sense of displacement is contradictory with the dextral sense of motion on the tear-faults. In summary, using classical conditions results in a decreasing gradient of slip in the transport direction and produces an incorrect sense of slip in the SW of our model. It is thus considered invalid, and it is necessary to include fault-slip constraints for improved restorations.

4.3. Restorations with geological constraints

4.3.1. Boundary conditions

Based on the results we obtained restoring the kinematic model, we focused our efforts on restoring the Niger Delta structure by specifying boundary wall displacements using the channel offsets. In this effort, two approaches to specify the geological boundary conditions have been adopted to restore the model. The channel offsets provide the total strike-slip at two locations in the model, but *a priori* we do not know whether the displacement should be partitioned between both sides of the bend, or assigned only to one side. This is important because the fault contacts are defined accordingly: if the displacement is assigned to one side only, then this side is defined as slave for the fault contact conditions, and the other side of the bend is the master and will not deform. In contrast, if the displacement is balanced on both sides of the major faults, then both sides of the faults move and are locally deformed to ensure the fault compliance. Ultimately, the relative displacement between the sidewalls where the conditions are set is the same, but the deformation that occurs to reach that amount of displacement is not. For both restorations, lateral walls are allowed to move only parallel to themselves and the restored horizon is the topmost horizon of the pregrowth strata (see Table 1 and Fig. 10). Here, the restoration is thus performed in one step, as only the pregrowth is restored.

To summarize, the restoration flattens the datum horizon and recovers the fault offset on the edges of the model, because these were set as constraints. Thus, in order to evaluate the restoration results, we need to analyze the patterns of slip on the faults and deformations that are in the interior of the model.

Table 1
Sets of boundary conditions used for the restorations.

	Flattening top surface	Lateral walls along normal	Strike-slip constraints	Contact on surfaces
Restoration 1	✓	✓	On one side	Slave/Master
Restoration 2	✓	✓	On both sides	Both sides move

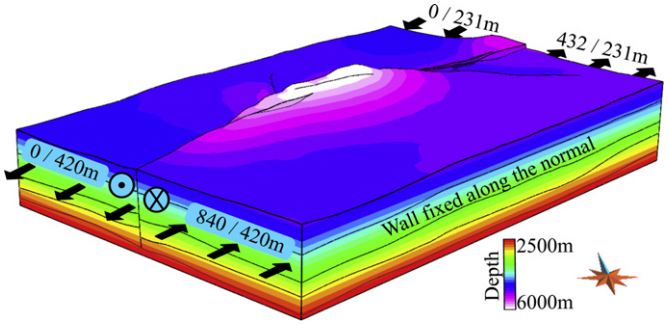

Fig. 10. Simplified model, showing the boundary conditions used for restorations 1 and 2. The top horizon is flattened and the lateral walls are fixed along their normal direction for both restorations. The numbers associated with the arrows on the model boundaries indicate the constrained amount of slip on each wall (the first number corresponds to restoration 1, the second to restoration 2). See also Table 1.

4.3.2. Slip profiles

One of the most effective ways to evaluate restorations of complex fault systems is by examining the displacement patterns of faults. Fault displacement patterns derived from successful restorations are, in turn, also one of the most useful restoration products as they can help to determine fault type, slip history, slip rate, and fault sealing capacity. Our restorations provide differential slip profiles, that allow assessing the magnitude of deformations on each fault. We have some knowledge about the expected displacements on these faults based on the horizon offsets. These were not used as constraints in the restoration (only offsets one the model boundaries were used) and thus we use the fault-slip patterns to analyze the validity of our restorations. It also provides insights into the fault kinematics in the bends, where the seismic data don't allow precise interpretations.

The strike- and dip-slip profiles on the restored horizon resulting from only one of the restorations (restoration 2 in Table 1) is shown in Fig. 11, the other restoration leading to very similar profiles (these profiles are plotted using relative displacements).

The strike-slip profile shows high variations along strike, from 250 m of summed slip to more than 900 m. Most of the strike-slip occurs on the tear-faults, while the thrusts and normal faults have very small components of horizontal slip. Moreover, outside of the bends, an increasing trend of slip in the transport direction is apparent, which is again consistent with their behavior as tear-faults.

The dip-slip profile highlights the presence of both restraining and releasing bends, with reverse displacements in the restraining bend and normal displacement in the releasing bend. The tear-faults appear to act as oblique thrusts in the restraining bend, and as oblique normal faults in the releasing bend. The dip-slip is more evenly distributed between the different types of faults than the strike-slip is. This highlights the fact that the shallow reverse and normal faults mostly accommodate local deformation due to the bends of the tear-faults, rather than the strike-slip motions of the tear-faults themselves.

These profiles suggests that strike- and dip-slip are effectively partitioned between the faults, as suggested by many authors for both analog models (McClay and Bonora, 2001; Mitra and Debapriya, 2011) and natural systems (see Biddle and Christie-Blick (1985) for a few examples). The geomechanical restoration approach is able to resolve this partitioning as a result of the fault geometry, fault cutoffs, and displacement boundary conditions. Thus, we suggest that geomechanical restorations using limited geological constraints can yield reasonable displacement patterns in complex fault systems.

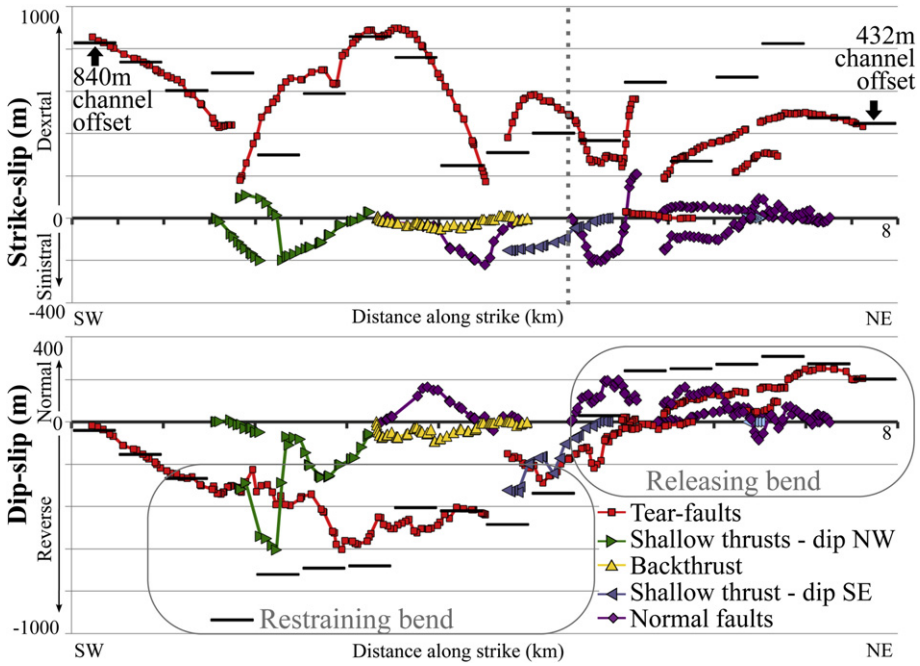

Fig. 11. Strike- and dip-slip (respectively horizontal and vertical components of the fault restoration vectors) for the faults within the model resolved by the geomechanical restoration. The black segments correspond to the sum of the average slip for every fault present on a 500 m distance along strike. Note that strike-slip is resolved principally on tear-faults, while the proper sense of dip-slip is resolved on thrust and normal faults within the structure.

4.3.3. Geometry of the restored models

One of the primary goals of restoration is to recover the geometry of tectonic and sedimentary structures at early stages in their development. This serves several purposes, but is mainly used to help assessing the timing of trap formation and reservoir evolution. In our case, the restored geometries also provide a way to evaluate the appropriateness of the boundary conditions. As shown on a NW–SE cross-section (Fig. 12), the geometry of the restored model is significantly different between our two restorations. Assigning the displacement on one wall only affects considerably the geometry of the faults, distorting them in an inconsistent way (Fig. 12-1). In contrast, balancing the displacement equally on each side of the major faults leads to a more consistent geometry, the shape of the faults being preserved while the blocks move (Fig. 12-2). Moreover, the underlying layers are almost flattened and show more consistent thicknesses with restoration 2 than with restoration 1. The backthrust offset is restored with restoration 2, while it shows a normal offset with restoration 1. These criteria highlight the fact that these restraining and releasing bends were probably generated with significant deformation occurring on both sides of the tear-faults. This is in contrast to the traditional view of deformation related to dip-slip faults, for which kinematic models typically have the majority of folding and other deformation localized in their hanging walls (see for instance Suppe (1983) or Groshong (2006)). Our results suggest that geomechanical restorations that allow for this partitioning of strain across faults are appropriate for natural systems such as strike-slip faults, where this deformation style is commonplace (Harding, 1985; Sylvester, 1988).

4.3.4. Deformation distribution

Besides the restoration vectors providing the slip profiles and restored geometry, another outcome of the restoration is the strain tensor, which is calculated for each tetrahedron in the model. As discussed in Section 2.1, we find it useful to analyze the significant invariants of the strain tensor, which can be computed from the restoration strains. Fig. 13 shows the computed dilation and distortion for both restorations.

The distortion is localized mostly close to the faults (Fig. 13-A1 and A2) and in the folded area of the uplift. This is consistent with the fact that the blocks are translated without significant distortion

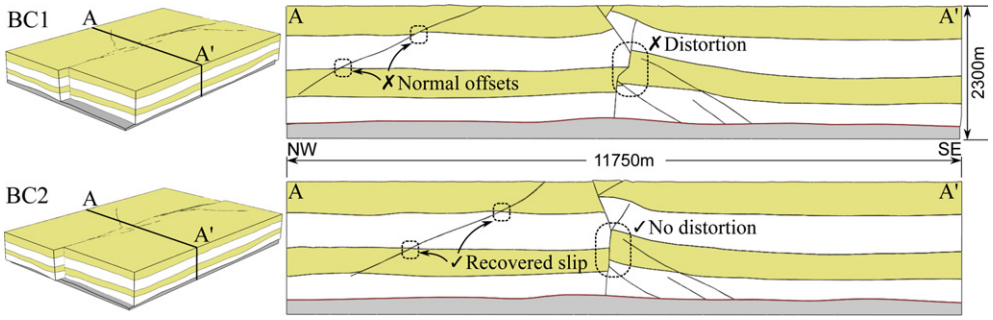

Fig. 12. Geometry of the restored model illustrated on a cross-section across the uplift in the restraining bend, with the sets of boundary conditions 1 and 2 (BC1 and BC2) as described in Table 1.

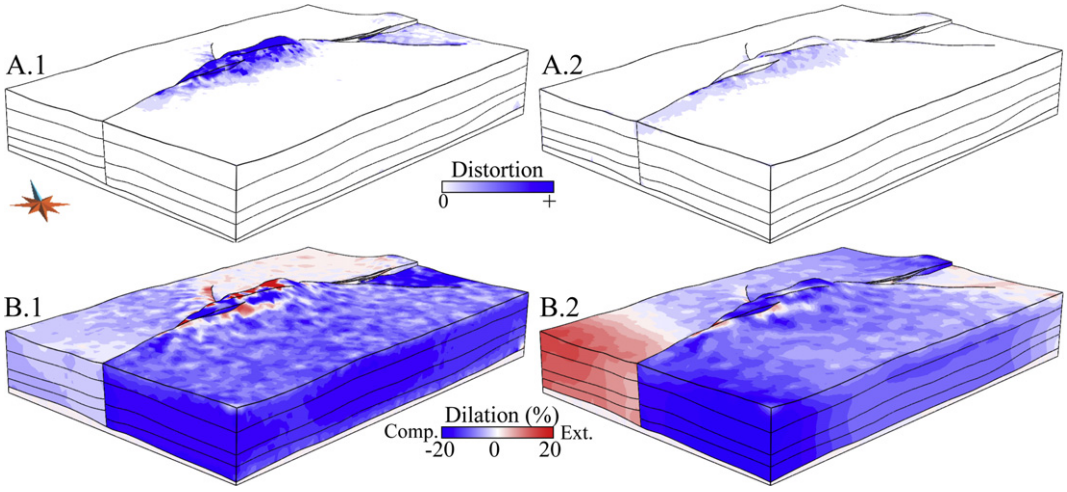

Fig. 13. Strain tensor invariants computed from the results of our two restorations (the boundary conditions are described in Table 1). A. Deviatoric distortion property; B. Dilation property. Ext. and Comp. stand respectively for model extension and compression in the tectonic sense.

except where the uplift deforms the structures. The distortion close to the faults is probably due to the roughness of their geometry. The higher values of distortion computed from restoration 1 are in agreement with the changes in shape of the faults that are observable in cross-section (Fig. 12).

The dilation distributions show high variations between the two restorations (Fig. 13-B1 and B2). In restoration 2, the dilation property shows gradients along strike, with inversed gradients on both sides of the bend: on the SE side of the tear-faults, it goes from retro-extension in the SW to retro-compression in the NE. This is consistent with the locations of the restraining and releasing bends. On the NW side of the bend, the dilation goes from retro-compression to retro-extension, and there is retro-extension at the backthrust location, as one would expect. In contrast, the dilation from restoration 1 shows relatively constant values everywhere but in the uplift, and there is no clear difference between the restraining and releasing bends.

This suggests again that partitioning of deformation on both sides of the fault is a more effective way of describing the styles of deformation along strike- and oblique-slip faults.

5. Conclusions

The 3D geomechanical restoration of a synthetic restraining bend model showed that using piercing points and/or additional displacement conditions in addition to flattening a deformed horizon is a promising approach for restoring strike- and oblique-fault systems, where classical boundary conditions fail to consistently recover viable patterns of slip and strain.

This new workflow was applied to restore a complex natural restraining bend system in the outer fold-and-thrust belt of the deep-water Niger delta basin. The high quality of the 3D seismic data allowed us to interpret in details the complex fault system and to identify channel offsets that are used to constrain the strike-slip along the major tear-faults of the system. We used these channels to constrain the restoration, and found that balancing displacement constraints equally on both side of the major faults, and allowing both sides of faults to deform, yielded the most reasonable restoration outcomes. The results show that we are able to resolve reasonable slip styles on the complex set of faults (strike-slip, normal, and thrust) that comprise the interior of the model, despite constraining slip only on model boundaries. This suggests that limited geologic fault slip constraints can be effectively incorporated in geomechanical restorations, yielding accurate restoration kinematics and forecasts of faults slip patterns within the structures. These restorations can be used to help validate interpretations of complex structures, and assess fault seal and hydrocarbon charge pathways based on fault slip histories.

Acknowledgments

This research work was performed within Harvard University. Chevron, ExxonMobil and Schlumberger are hereby acknowledged for their financial support. Paradigm is acknowledged for providing the Gocad software, and the Gocad Research Group/Lorraine Université for RestorationLab (3D geomechanical restoration plugin) and StructuralLab (implicit modeling plugin). Landmark's University Grant Program made available to Harvard University the seismic interpretation software that was used in this study. We would like to thank Ian Edwards (Dolphin Geophysical) for helping to facilitate this research, and Guillaume Caumon and Sankar Muhuri for providing constructive reviews that helped improve this paper.

Appendix A. Supplementary data

Supplementary data related to this article can be found at http://dx.doi.org/10.1016/j.jsg.2012.12.009.

References

Benesh, N., 2010. The Mechanics of Fault-Bend Folding and Tear-Fault Systems in the Niger Delta. PhD thesis. Harvard University, Cambridge, USA, 124 pp, .
Biddle, K., Christie-Blick, N., 1985. Strike-slip Deformation, Basin Formation, and Sedimentation. In: SEPM Special Publication, vol. 37.
Bilotti, F., Shaw, J.H., 2005. Deep-water Niger Delta fold and thrust belt modeled as a critical-taper wedge: the influence of elevated basal fluid pressure on structural styles. AAPG Bulletin 89 (11), 1475–1491.
Caumon, G., Antoine, C., Tertois, A.-L., 2007. Building 3D geological surfaces from field data using implicit surfaces. In: Proceedings: 27th Gocad Meeting, Nancy, France, pp. 1–6.
Chamberlin, R.T., 1910. The Appalachian folds of central Pennsylvania. Journal of Geology 18 (3), 228–251.
Connors, C.D., Denson, D.B., Kristiansen, G., Angstadt, D.M., 1998. Compressive anticlines of the mid-outer slope, central Niger Delta (abs.). In: AAPG Annual Convention, Rio de Janeiro, Brasil.
Corredor, F., Shaw, J.H., Bilotti, F., 2005. Structural styles in the deep-water fold and thrust belts of the Niger Delta. AAPG Bulletin 89 (6), 753–780.
Dahlstrom, C.D.A., 1969. Balanced cross sections. Canadian Journal of Earth Sciences 6, 743–757.

De Santi, M.R., Campos, J.L.E., Martha, L.F., 2002. A finite element approach for geological section reconstruction. In: Proceedings: 22nd Gocad Meeting, Nancy, France, pp. 1–13.

Doust, H., Omatsola, E., 1990. Niger Delta in divergent/passive margin basins. In: Edwards, J.D., Santogrossi, P.A. (Eds.), Divergent/passive Margin Basins. AAPG Memoir, vol. 48, pp. 201–238.

Durand-Riard, P., 2010. Gestion de la complexité géologique en restauration géomécanique 3D. PhD thesis. Institut Polytechnique National de Lorraine, Nancy, France, 150 pp, .

Durand-Riard, P., Caumon, G., Muron, P., 2010. Balanced restoration of geological volumes with relaxed meshing constraints. Computers & Geosciences 36 (4), 441–542.

Durand-Riard, P., Salles, L., Ford, M., Caumon, G., Pellerin, J., 2011. Understanding the evolution of syn-depositional folds: coupling decompaction and 3D sequential restoration. Marine and Petroleum Geology 28 (8), 1530–1539.

Durand-Riard, P., Shaw, J., 2012. Insights into the regional evolution of the outer fold-and-thrust belt, Niger Delta, from combining new techniques in 3D sequential geomechanical restoration with decompaction. In: American Association of Petroleum Geologists Annual Convention, Programs with Abstracts, Long Beach, CA.

Frank, T., Tertois, A.-L., Mallet, J.-L., 2007. 3D reconstruction of complex geological interfaces from irregularly distributed and noisy point data. Computers & Geosciences 33 (7), 932–943.

Gratier, J.P., Guillier, B., 1993. Compatibility constraints on folded and faulted strata and calculation of total displacement using computational restoration (UNFOLD program). Journal of Structural Geology 15 (3–5), 391–402.

Groshong, R.H., 2006. Structural validation, restoration and prediction. In: 3D Structural Geology: A Practical Guide To Surface And Subsurface Map Interpretation. Springer Verlag, Berlin Heidelberg, pp. 305–372.

Guzofski, C., Müeller, J., Shaw, J.H., Muron, P., Medwedeff, D., Bilotti, F., Rivero, C., 2009. Insights into the mechanisms of fault-related folding provided by volumetric structural restorations using spatially varying mechanical constraints. AAPG Bulletin 93, 479–502.

Harding, T.P., 1985. Seismic characteristics and identification of negative flower structures, positive flower structures, and positive structural inversion. AAPG Bulletin 69, 582–600.

Lovely, P.J., 2011. Fault-Related Deformation Over Geologic Time: Integrating Field Observations, High Resolution Geospatial Data And Numerical Modeling To Investigate 3d Geometry And Non-Linear Material Behavior. PhD thesis. Stanford University, Stanford, USA, 265 pp.

Lovely, P.J., Pollard, D., Flodin, E., Guzofski, C., Maerten, F., 2010. Pitfalls among the promises of mechanics based structural restoration. In: American Association of Petroleum Geologists Annual Convention, Programs with Abstracts, Neworleans, Louisiana, USA.

Maerten, L., Maerten, F., 2006. Chronologic modeling of faulted and fractured reservoirs using geomechanically based restoration: technique and industry applications. AAPG Bulletin 90 (8), 1201–1226.

Massot, J., 2002. Implémentation de méthodes de restauration équilibrée 3D. PhD thesis. Institut Polytechnique National de Lorraine, Nancy, France, 157 pp.

McClay, K., Bonora, M., 2001. Analog models of restraining stepovers in strike-slip fault systems. AAPG Bulletin 85 (2), 233–260.

Mitra, S., Debapriya, P., 2011. Structural geometry and evolution of releasing and restraining bends: insights from laser-scanned experimental models. AAPG Bulletin 95 (7), 1147–1180.

Moretti, I., Lepage, F., Guiton, M., 2006. Kine3D: a new 3D restoration method based on a mixed approach linking geometry and geomechanics. Oil & Gas Science and Technology 61 (2), 277–289.

Müeller, J., Guzofski, C., Rivero, C., Plesch, A., Shaw, J., Bilotti, F., Medwedeff, D., 2005. New approaches to 3D structural restoration in fold-and-thrust belts using growth data. In: American Association of Petroleum Geologists Annual Convention, Programs with Abstracts, Calgary, Canada.

Muron, P., 2005. Méthodes numériques 3D de restauration des structures géologiques faillées. PhD thesis. Institut Polytechnique National de Lorraine, Nancy, France, 145 pp.

Oakley, D., Knight, N., 1995. Adaptive dynamic relaxation algorithm for non-linear hyperelastic structures part I. formulation. Computer Methods in Applied Mechanics and Engineering 126 (1–2), 67–89.

Papadrakakis, M., 1981. A method for the automatic evaluation of the dynamic relaxation parameters. Computer Methods in Applied Mechanics and Engineering 25 (1), 35–48.

Plesch, A., Shaw, J., Kronman, D., 2007. Mechanics of low-relief detachment folding in the Bajiaochang field, Sichuan basin, China. AAPG Bulletin 91 (11), 1559–1575.

Plesch, A., Shokair, K., Shaw, J., 2010. 3D finite-element based structural restorations used to constrain fault and fracture patterns: examples from synthetic models and the Middle East. In: Proceedings 30th Gocad Meeting, Nancy, France, pp. 1–8.

Rouby, D., 1994. Restauration en carte des domaines faillés en extension. PhD thesis, Université de Rennes I, Rennes, France, 210 pp.

Rouby, D., Xiao, H., Suppe, J., 2000. 3-D restoration of complexly folded and faulted surfaces using multiple unfolding mechanisms. AAPG Bulletin 84 (6), 805–829.

Shaw, J., Bischke, R., Suppe, J., 1994. Relations between folding and faulting in the Loma Prieta epicentral zone: strike-slip fault-bend folding. In: Simpson, R.W. (Ed.), The Loma Prieta, California, Earthquake of October 17, 1989. U.S. Geological Survey Professional Paper, vol. 1550-F, pp. 3–22.

Suess, M., Plesch, A., Shaw, J., Zahran, M., 2009. Paleostrain and fracture potential of deep-seated wrench-fault systems in the Post-Hith of Block 11 (Qatar). In: International Petroleum Technology Conference, Program with Abstracts, Doha, Qatar.

Suppe, J., 1983. Geometry and kinematics of fault-bend folding. American Journal of Science 283 (7), 684–721.

Sylvester, A.G., 1988. Strike-slip faults. Geological Society of America Bulletin 100 (11), 1666–1703.

Titeux, M.-O., 2009. Restauration et incertitudes structurales: changements d'échelles des propriétés mécaniques et gestion de la tectonique salifère. PhD thesis, Institut Polytechnique National de Lorraine, Nancy, France, 145 pp.

Underwood, P., Park, K.C., 1978. Implementation of a variable-step integration technique for non-linear structural dynamic analysis. Methods for Structural Analysis, M, 1–12.

Vidal-Royo, O., Cardozo, N., Muñoz, J.A., Hardy, S., Maerten, L., 2011. Multiple mechanisms driving detachment folding as deduced from 3d reconstruction and geomechanical restoration: the Pico del Águila anticline (External Sierras, Southern Pyrenees). Basin Research 23, 1–19.

Wriggers, P., 2002. Computational Contact Mechanics. Wiley, Chichester. 441pp.

Wu, S., Bally, A.W., 2000. Slope tectonics - comparisons and contrasts of structural styles of salt and shale tectonics of the northern Gulf of Mexico with shale tectonics of offshore Nigeria in Gulf of Guinea. In: Mohriak, W., Talwani, M. (Eds.), Atlantic Rifts and Continental Margins. Geophysical Monograph, vol. 115. American Geophysical Union, pp. 151–172.

Zienkiewicz, O., 1977. The Finite Element Method, third ed. McGraw-Hill, London. 787pp.